# Control system design and Stability Analysis for a three phase SiC-based Filter-less Grid-connected PV Inverter

Yanjun Shi, *Senior Member, IEEE*, Lu Wang, *Student Member, IEEE*, Hui Li, *Senior Member, IEEE*
The Center for Advanced Power Systems, Florida State University
Tallahassee, Florida, 32304
yshi3@fsu.edu

***Abstract*— In this paper, a control system of a filter-less grid-connected SiC inverter is designed. Stability analysis has been researched with a focus on grid disturbance rejection. The analysis shows that the conventional control method with instantaneous grid voltage feedforward (IGVF) will significantly limit the bandwidth or stability margin of a filter-less grid-connected inverter, thus make the inverter sensitive to grid disturbance. Two proposed grid voltage feedforward control methods, which require little additional computation resources, are presented to suppress the grid voltage disturbance. The design methods of control parameters are derived. The effects of the proposed feedforward methods are also compared with that of conventional IGVF. Finally, the grid-connected experimental results of a three phase SiC based filter-less PV inverter are provided to verify and compare the proposed control methods.**

***Keywords*— *Inverter; grid-connected; Silicon carbide MOSFET; Filter-less; stability.***

## I. INTRODUCTION

Grid-connected inverter designers are making continuous efforts to reduce the size, weight, cost, power loss, and failure rate of the grid interface filters [1]-[4]. A grid interface filter, or line filter, is the filter connected at the AC side of a voltage-source converter (VSC) to suppress the switching frequency current ripple. It is often costly and consumes a large portion of power loss, weight, and size in a grid connected inverter, especially in medium to high power applications. A commonly recognized method to reduce the size and weight of a grid interface filter is to increase the order of a filter, so that less inductance is required. However, these higher-order power filters, including LCL filters, contain one or multiple resonant peaks which require passive or active damping. Passive damping leads to extra power loss and reduces filter attenuation [5], [6]. Active damping requires extra sensors and/or extra computation power, and their effects are often limited by digital control delay and parameter uncertainty [7]-[9].

This paper proposes to completely remove the grid interface filter by utilizing WBG device and multilevel technology. The feasibility of connecting a three phase SiC filter-less PV inverter to the grid is analyzed and experimentally demonstrated. Several important aspects of the proposed filter-less grid-connected control are investigated including effects of grid voltage feedforward (GVF); extra control delay introduced by an anti-EMI-noise filter and its influence on voltage feedforward; limited computation resources due to high switching frequency; as well as the effect of grid impedance variation on system stability and performance. Two grid voltage feedforward (GVF) control methods, referred as fundamental frequency grid voltage feedforward (FFGVF) and frequency limited grid voltage feedforward (FLGVF), which require little additional computation resources, is proposed to suppress the grid voltage disturbance. The effects of the two proposed GVF methods are also compared with that of conventional instantaneous grid voltage feedforward (IGVF). Finally, the grid-connected experimental results are presented for the 5-level grid-connected PV inverter prototype.

## II. TOPOLOGY AND CONTROL SYSTEM

The topology of the PV converter is shown in Fig.1. This inverter consists of six 1200 V SiC T-type modules provided by Wolfspeed. Every two modules are parallel-coupled through an inter-cell transformer (ICT).The carriers of the paralleled modules in each phase are interleaved to form a five-level line-to-neutral output voltage. The output of the ICTs are directly connected to the load or the utility grid, thereby in this paper, this PV inverter is referred as a filter-less inverter. More details of the operation principle of this topology have been presented

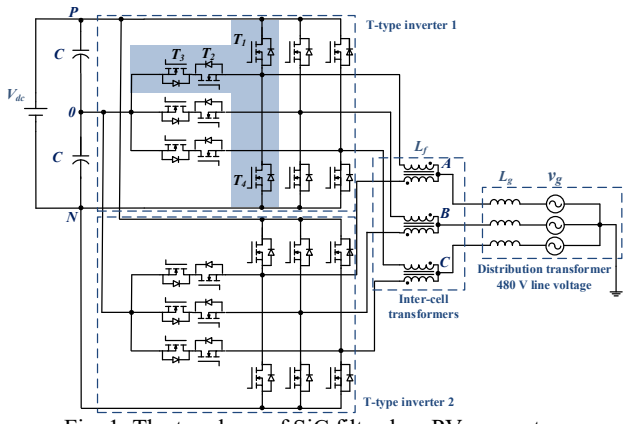


Fig. 1. The topology of SiC filter-less PV converter.

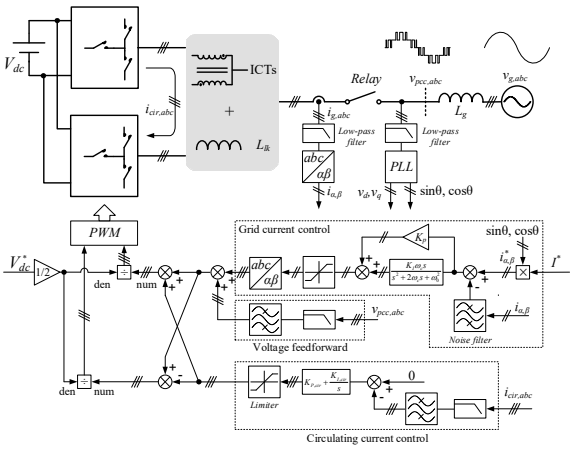


Fig. 2 The control system configuration of the filter-less inverter.

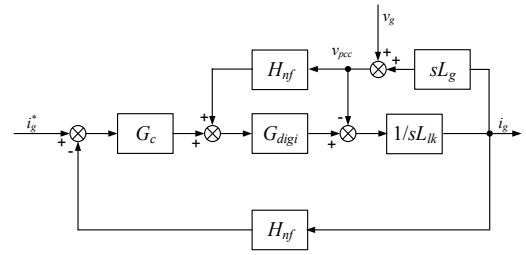

(a)

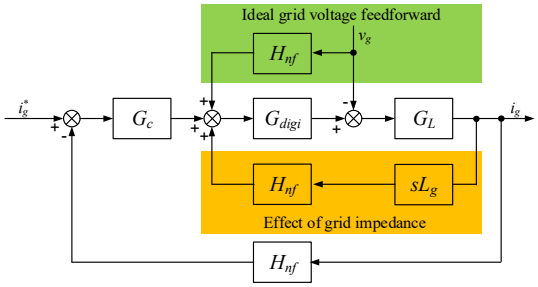


(b)

Fig. 3. Control block diagram of current loop with grid voltage feedforward. (a) Original form; and (b) Equivalent form.

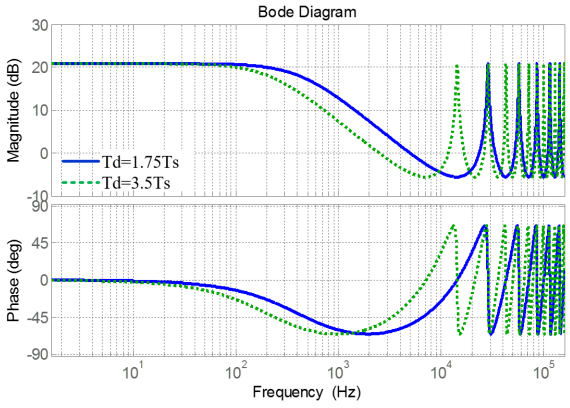


Fig. 4. Bode plot of $G_{VF}$ when $L_g = 10L_{lk}$.

in [10]. The developed control system is shown in Fig. 2. $L_g$ is the grid inductance including distribution transformer leakage inductance and power cable inductance, $L_{lk}$ is the total parasitic inductance of the inverter. In this research, $L_g$ is at least 10 times larger than $L_{lk}$.

The grid current controller is a proportion-resonant (PR) controller in stationary frame. Due to limited computation resource, it is not feasible to avoid alias and noise by controlling the sample time. Therefore, there is an analog anti-alias low pass filter and a digital noise filter implemented in the grid current sampling loop. The output line-to-line voltage of this PV inverter is a seven-level staircase voltage instead of the sinusoidal voltage in conventional inverters, a low-pass filter is required after the voltage sensor to filter out the switching harmonic of output voltage. A circulating current control is applied to reject the dc circulating current between two windings of the ICT. As the inductor windings are tightly coupled, the circulating current is much smaller than the fundamental current. A two-channel differential current sensor is preferred to ensure accuracy on circulating current control. If the two-winding inductance of the ICT is identical, the circulating current control loop will be decoupled from phase current control.

Fig. 3 (a) shows the current loop control block diagram, in which $i_g$ is the grid current, and $G_c$ is the transfer function of the current loop PR controller. Ideally, the grid voltage $v_g$ should be used in the feedforward control since it reveals the true disturbance from the grid. However, only inverter output voltage $v_{pcc}$ can be sensed in a real application. In a filter-less inverter, $v_{pcc}$ is strongly influenced by the inverter output current. In this case, the grid voltage feedforward control can affect stability. This can be explained with Fig. 3 (b). Fig. 3 (b) is an equivalent form of Fig. 3(a), with $G_L = 1/sL$ where $L = L_{lk} + L_g$ is the total inductance. It can be observed in Fig. 3 (b) that the existence of $L_g$ creates a positive feedback loop which can decrease the stability margin. The loop gain of this positive feedback is:

$$k = \left|sL_g G_{digi} G_L H_{nf}\right| = \left|\frac{L_g}{L} e^{-3.5T_s \cdot s}\right| = \frac{L_g}{L_{lk} + L_g} = \frac{L_g}{L} \quad (1)$$

The value of $k$ is between zero (ideal grid) and one (zero inverter parasitic inductance). In this research, $k \in [0.9,1)$. Therefore, this positive feedback loop will not necessarily make the system unstable since the loop gain is still smaller than one. But its phase delay can influence system phase margin.

The open-loop transfer function of grid current control **with** grid voltage feedforward can be derived as:

$$G_{LP\_VF} = \frac{G_c G_d G_L}{1 - kG_d} = G_{LP} \cdot \frac{1}{1 - kG_d} = G_{LP} \cdot G_{VF} \quad (2)$$

where $G_{LP\_VF}$ can be seen as $G_{LP}$ cascaded with a low-pass filter $G_{VF} = 1/(1 - kG_d)$. $G_{VF}$ gives the control loop an extra dc gain of $1/(1-k)$. It also introduced a significant phase lag around 1 kHz, as shown in Fig. 4. Fig. 4 and (2) also show that, although the digital control delay is relatively small in the SiC-base inverter, however, the effect of the delay in a filter-less inverter is shifted to a much lower frequency at the kHz range.

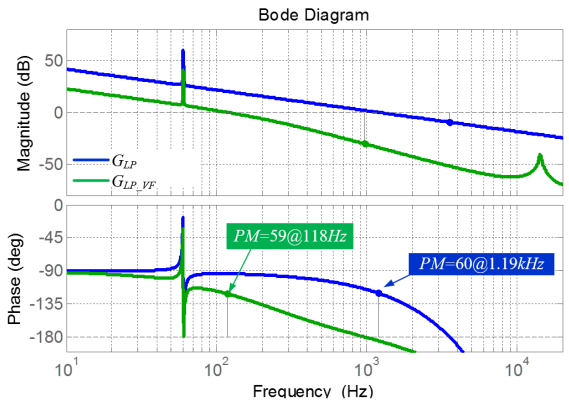

Fig. 5. Open-loop bode plot of system w/ and w/o a grid voltage feedforward

Fig. 5 presents the open-loop bode plot of the grid current control with and without grid voltage feedforward under the same phase margin. In a filter-less inverter, with grid voltage feedforward, the maximum crossover frequency is reduced to about 1/10.

## III. PROPOSED CONTROL METHODS AND STABILITY ANALYSIS

A major challenge of controlling a filter-less inverter is that the PCC voltage is largely influenced by the inverter own dynamic instead of the grid voltage dynamic. As a result, the conventional way of instantaneous grid voltage feedforward (IGVF) will cause instability. To solve this issue, two control methods, referred as Fundamental frequency grid voltage feedforward (FFGVF) and Frequency limited grid voltage feedforward (FLGVF) are proposed.

### *A. Fundamental Frequency Grid Voltage Feedforward (FFGVF)*

A simple solution to solve this issue is to only feedforward the fundamental frequency component of grid voltage, as shown in Fig. 6, where the d-axis voltage $v_d$ generated from PLL is feeding into a moving average filter (MAF), and then is fed into a reverse $dq$ transformation to generate the three-phase voltage that only contains the fundamental frequency of the grid voltage. Since this algorithm uses the output of PLL algorithm, its time penalty is the update time of MAF. In this research, updating MAF costs 5 extra CPU cycles, while the total CPU cycles in the interruption is 3000.

The control block diagrams of the current control loop under the FFGVF control is shown in Fig. 7. Comparing Fig. 3 and Fig. 7, FFGVF control doesn't introduce the positive feedback loop, thereby it will not influence the stability of the inverter, meanwhile, it can still prevent over current during the start-up, or over modulation when the grid voltage changes; and make the control loop less sensitive to noise. At frequency above fundamental frequency, FFGVF is equivalent to no grid feedforward. Therefore, this control method has a good control-to-output bandwidth, but limited disturbance rejection capabilityThe performance of FFGVF is compared with that of conventional instantaneous grid voltage feedforward (IGVF)

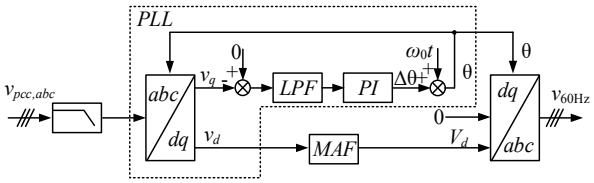

Fig. 6. Control schematic of proposed FFGVF.

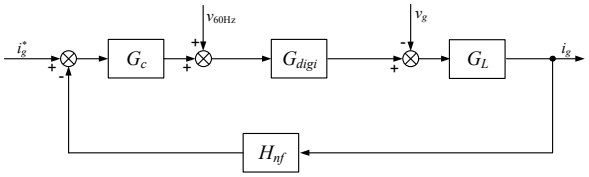

Fig.7. Current loop control block diagram with FFGVF control.

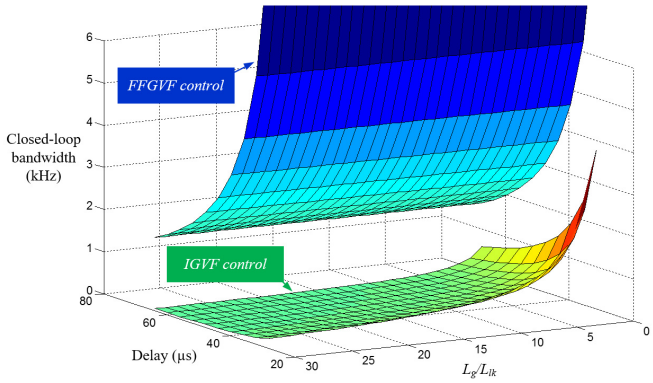

Fig.8. Closed-loop bandwidth of conventional instantaneous grid voltage feedforward (IGVF) and fundamental frequency grid voltage feedforward (FFGVF) at different time delay and grid inductance.

System closed-loop bandwidth can be calculated for IGVF and FFGVF methods under different time delay $T_d$ and $L_g/L_{lk}$ ratio. Fig. 8 is a 3D plot of closed-loop bandwidth at different time delay and $L_g/L_{lk}$ ratio for IGVF and FFGVF. It can be seen that IGVF has significantly decreased closed-loop bandwidth, especially at weaker grid. With grid voltage feedforward, maximum closed-loop bandwidth is influenced by both $T_d$ and $L_g/L_{lk}$ ratio. And when the grid is weak enough, the difference among different $T_d$ is less important. And maximum closed-loop bandwidth is not influenced by grid impedance under FFGVF control.

### *B. Frequency Limited Grid Voltage Feedforward (FLGVF)*

To improve disturbance rejection capability while maintaining the control bandwidth achieved by FFGVF, another control method, referred as frequency limited grid voltage feedforward (FLGVF), is proposed. The control block diagram of FLGVF is the same as the one in Fig. 3. The difference is in the design of the low-pass filter after the grid voltage sampling. In the original design of Fig. 3, the low-pass filter is used to suppress the carrier frequency harmonics, which is at 100 kHz. In the FLGVF control, the cutoff frequency of the low-pass filter is designed to be much lower, so that only low-frequency part of the grid voltage is sampled. The transfer function and cutoff frequency of the low-pass filter are given by (3):

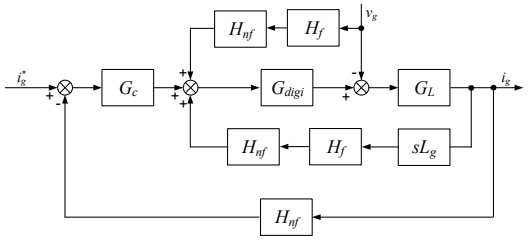


Fig. 9. Current loop control block diagram with FLGVF control

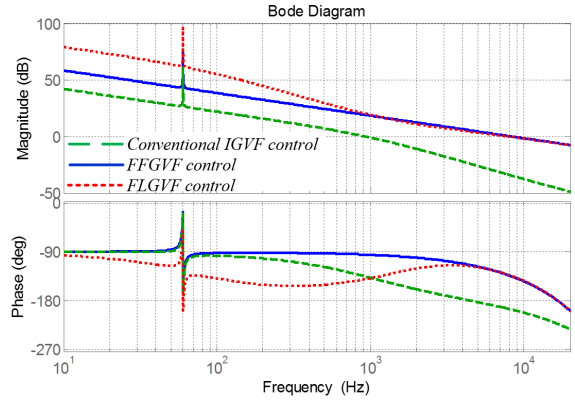


Fig. 10. Open-loop bode plot of the reference-to-output transfer functions under IGVF, FFGVF and FLGVF control.

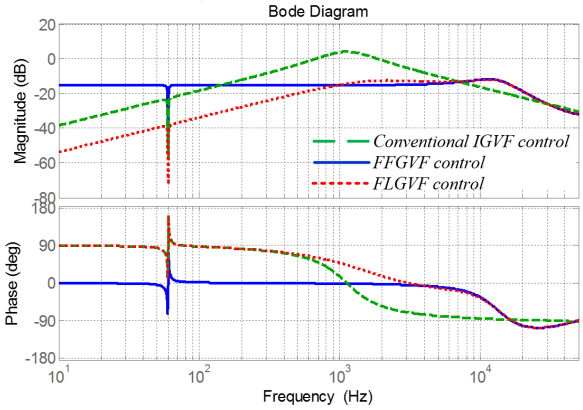


Fig. 11. Bode plot of the disturbance-to-output transfer functions under IGVF, FFGVF and FLGVF.

$$\begin{cases} H_f = \dfrac{\omega_f}{s+\omega_f} \\ \omega_f = \dfrac{\frac{\pi}{2} - PM - \sin^{-1}[k\cos(PM)]}{T_d} \end{cases} \quad (3)$$

This low pass filter can be realized by modifying the parameters of the analog filter in the voltage sampling circuit. Therefore, it doesn't have computation time penalty. The control block diagram of grid current loop with FLGVF control is shown in Fig.9. Fig. 10 is the open-loop bode plots of the reference-to-output transfer function under IGVF, FFGVF, and FLGVF control when L_g=10L_lk= 100 μH, and PM = 45°. The FFGVF and FLGVF have the same parameters for current control loop. It shows that FLGVF control can increase the phase angle near the crossover frequency, thereby it provides same control bandwidth as FFGVF control. . The advantage of FLGVF over FFGVF can be demonstrated in Fig. 11, which is the bode plot of disturbance-to-output transfer function. It shows that FLGVF has better disturbance rejection than FFGVF at frequency below 1 kHz.

## IV. EXPERIMENT RESULTS

The 60kW SiC filter-less inverter laboratory prototype is shown in Fig. 12. The input of the prototype is a 150 kW DC power supply; the output of the PV inverter is connected to a 480V/4.16kV 1.5 MW transformer, through about 35 meters of AWG 0 cable. The measured total grid inductance is 120μH, which is 12 times of the total parasitic inductance of the inverter.

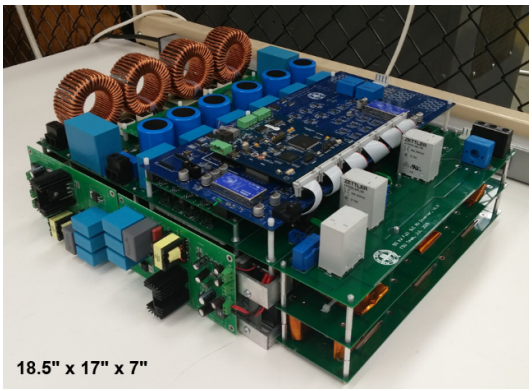


Fig. 12. The SiC Filter-less PV inverter prototype.

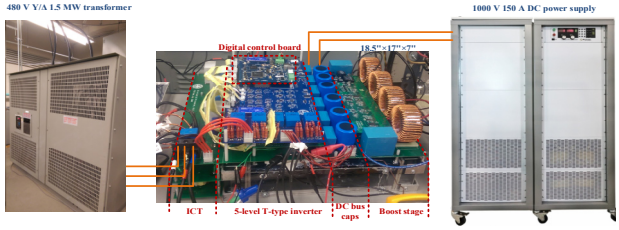


Fig. 13. The SiC 5LT$^2$ PV inverter prototype.

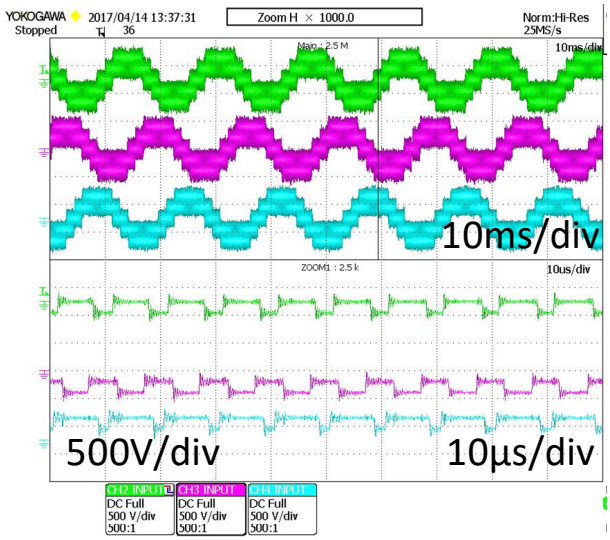


Fig. 14 Three phase output line-to-neutral voltage.

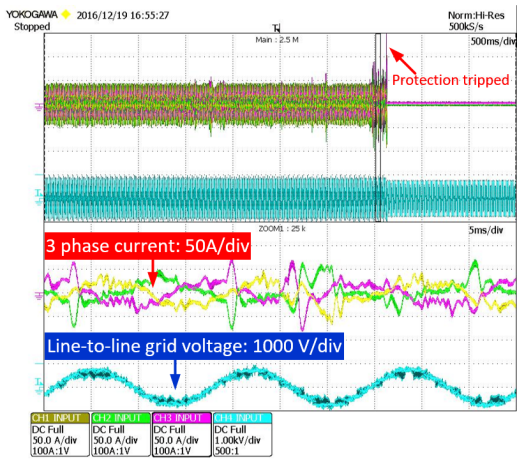


Fig.15. PV inverter output current and grid voltage under IGVF control.

Three grid connected experiments were performed applying FFGVF, FLGVF, and IGVF, respectively. The experiment setup is shown in Fig. 13. In all three experiments, the grid current reference was set to be 72 A RMS. The voltage measured at PCC point is a five-level line to neutral voltage waveform, as shown in Fig. 14.

In the first experiment, the control performance of conventional IGVF was tested. As shown in Fig. 15, the PV inverter can maintain grid connected operation for several seconds, but with large harmonic current components and fundamental current error. After several seconds of running, the inverter became unstable and protections were tripped.

In the second experiment, the control performance of FFGVF was tested. The results are shown in Fig. 16. When FFGVF is applied, the fundamental frequency component of $v_{pcc}$ is extracted with a proposed control method, and used as feedforward for the current control loop. Under FFGVF control, the grid voltage feedforward has no effect on grid voltage harmonic rejection, but it allows the control bandwidth to be extended to above 1 kHz. However, the grid voltage harmonic rejection ability of FFGVF is provided by the grid impedance and the controller gain. Therefore, FFGVF has poor attenuation for low frequency harmonics. Fig. 15 (b) displays FFT result of phase A current under FFGVF control as 3.54%, and there are observable low frequency harmonics containing third harmonic portion.

A third experiment was conducted to evaluate the control performance of FLGVF. The results are presented in Fig. 17. It can be observed that the current distortion of Fig. 17 is reduced with THD of 2.31% comparing with the waveforms in Fig. 16. When comparing Fig. 16 with Fig. 17, one significant difference is that the low frequency harmonics are reduced. This can be explained with Fig. 11: Although FLGVF has the same control bandwidth compared with FFGVF, it provides additional capacitive attenuation towards grid voltage disturbance at low frequency. At higher frequency, both FLGVF and FFGVF have same control performance.

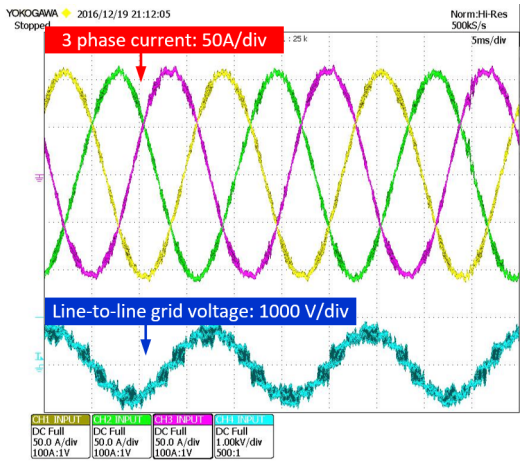


(a)

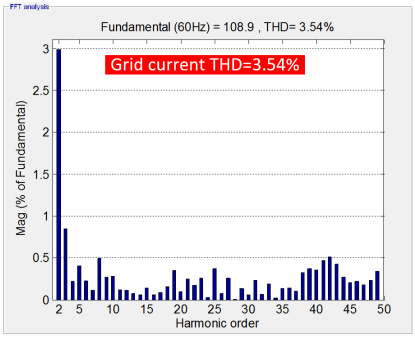


(b)

Fig. 16. PV inverter grid-connected experiment results under FFGVF control. (a) Three-phase output current and line-to-line voltage at PCC; and (b) FFT result of phase A output current.

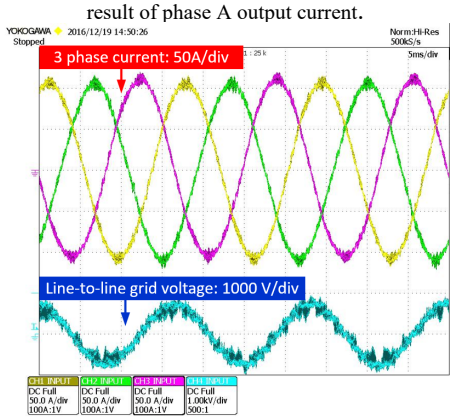


(a)

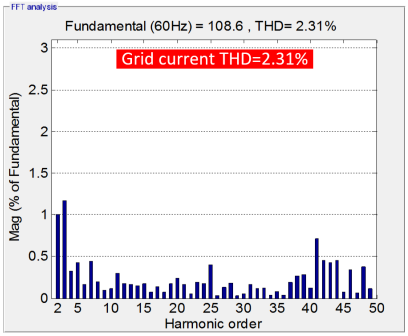


(b)

Fig. 17. PV inverter grid connected experiment results under FLGVF control. (a) Three-phase output current and line-to-line voltage at PCC; and (b) FFT result of phase A output current.

## V. CONCLUSIONS

In this paper, the feasibility of connecting a three phase SiC filter-less PV inverter to the grid is analyzed and experimentally demonstrated. Two grid voltage feedforward control methods to suppress the grid voltage disturbance are compared. Experimental results are presented for a 60 kW two-stage grid-connected PV inverter prototype using 1200 V SiC T-type MOSFET modules switched at 50 kHz. The designed prototype has a power density of 27 W/in3 and 3 kW/kg, a peak efficiency of 99.2%, and a CEC efficiency of 99.0%. Grid connected experiments were performed for three GVF methods, with grid inductance being 12 times of the inverter total parasitic inductance. The measured current THD for FFGVF and FLGVF are 3.54% and 2.31%, respectively. Following conclusions can be drawn from the analysis and experimental results:


## ACKNOWLEDGMENT

The information, data, or work presented herein was funded in part by the Office of Energy Efficiency and Renewable Energy (EERE), U.S. Department of Energy, under Award Number DE-EE0006521 with North Carolina State University, PowerAmerica Institute.




## REFERENCES


[1] K. Jalili and S. Bernet, "Design of LCL Filters of Active-Front-End Two-Level Voltage-Source Converters," IEEE Trans. on Ind. Electron., vol. 56, no. 5, pp. 1674-1689, May 2009.

[2] P. Channegowda and V. John, "Filter Optimization for Grid Interactive Voltage Source Inverters," IEEE Trans. on Ind. Electron., vol. 57, no. 12, pp. 4106-4114, Dec. 2010.

[3] G. Gohil, L. Bede, R. Teodorescu, T. Kerekes and F. Blaabjerg, "Line Filter Design of Parallel Interleaved VSCs for High-Power Wind Energy Conversion Systems," IEEE Trans. on Power Electron., vol. 30, no. 12, pp. 6775-6790, Dec. 2015.

[4] E. Kantar and A. M. Hava, "Optimal Design of Grid-Connected Voltage-Source Converters Considering Cost and Operating Factors," IEEE Trans. on Ind. Electron., vol. 63, no. 9, pp. 5336-5347, Sept. 2016.

[5] R. Peña-Alzola, M. Liserre, F. Blaabjerg, R. Sebastián, J. Dannehl and F. W. Fuchs, "Analysis of the Passive Damping Losses in LCL-Filter-Based Grid Converters," IEEE Trans. on Power Electron., vol. 28, no. 6, pp. 2642-2646, June 2013.

[6] A. A. Rockhill, M. Liserre, R. Teodorescu and P. Rodriguez, "Grid-Filter Design for a Multimegawatt Medium-Voltage Voltage-Source Inverter," IEEE Trans. on Ind. Electron., vol. 58, no. 4, pp. 1205-1217, April 2011.

[7] X. Wang, F. Blaabjerg and P. C. Loh, "Grid-Current-Feedback Active Damping for LCL Resonance in Grid-Connected Voltage-Source Converters," IEEE Trans. on Power Electron., vol. 31, no. 1, pp. 213-223, Jan. 2016.

[8] C. Bao, X. Ruan, X. Wang, W. Li, D. Pan and K. Weng, "Step-by-Step Controller Design for LCL-Type Grid-Connected Inverter with Capacitor–Current-Feedback Active-Damping," IEEE Trans. on Power Electron., vol. 29, no. 3, pp. 1239-1253, March 2014.

[9] J. Dannehl, F. W. Fuchs, S. Hansen and P. B. Thogersen, "Investigation of Active Damping Approaches for PI-Based Current Control of Grid-Connected Pulse Width Modulation Converters With LCL Filters," IEEE Trans. on Ind. Appl., vol. 46, no. 4, pp. 1509-1517, July-Aug. 2010.

[10] Y. J. Shi, L. Wang, R. Xie, Y. X. Shi, and H. Li, "A 60kW 3kW/kg 5-Level T-Type SiC PV inverter with 99.2% peak Efficiency," IEEE Trans. on Ind. Electron., Early Access Articles, 2017


.